

Predicting multidimensional distributive properties of hyperbranched polymer resulting from AB_2 polymerization with substitution, cyclization and shielding

I. Kryven^{a,*}, P. D. Iedema^a

^a*University of Amsterdam, Science Park 904,
1098 XH Amsterdam, The Netherlands*

Abstract

A deterministic mathematical model for the polymerization of hyperbranched molecules accounting for substitution, cyclization, and shielding effect has been developed as a system of nonlinear population balances. The solution obtained by a novel approximation method shows perfect agreement with the analytical solution in limiting cases and provides, for the first time in this class of polymerization problems, full multidimensional results.

Keywords: Chain length distribution, Hyperbranched polymer, Convolution, Substitution, Cyclization, Shielding

2000 MSC: 80A30, 82D60

Contents

1	Graph representation for hyperbranched polymers	4
2	Reaction mechanisms and mathematical model	6
2.1	Numerical treatment	11
2.2	The numerical algorithm	16
3	Results and post-analysis	17
3.1	Time dependent scalars	20

*Corresponding author

Email addresses: i.kryven@uva.nl (I. Kryven), p.d.iedema@uva.nl (P. D. Iedema)

3.2	1-dimensional distributions	22
3.3	2-dimensional distributions	28
3.4	Dynamic evolution of 2D distributions	30
4	Non-linear substitution as a consequence of shielding	32
5	Appendix 1	38

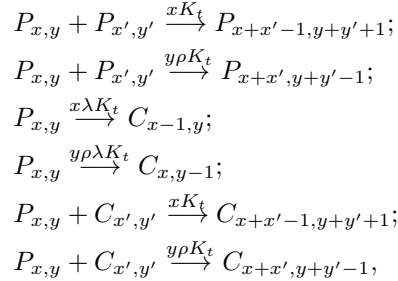
Introduction

In this paper the mathematical modelling of hyperbranched polymers based on monomers of the AB_2 type is taken at hand, allowing the calculation of various microstructural properties, using a numerical-mathematical scheme based on a graph-theoretical description of branching topology. . In previous work, scalar quantities like average molecular weight, polydispersity, degree of branching, or gel point have been successfully predicted. These results were mainly achieved either by statistical theories of Stockmayer [1, 2] and Flory [3] or, later, by stochastic simulations [4] and a generating functions approach [5, 6, 7]. Most theoretical models that describe the polymerization of AB_2 monomer are based on the assumption that all functional groups of the same type are equally reactive, and react independently of one another. In other words, all B groups in the AB_2 monomer units in the polymer have the same reactivity. Yet, the equal reactivity is questioned if a *substitution* effect is taken into account [6].

As regards the AB_2 problem with substitution, significant progress has been achieved in studies by Galina[5, 8], Cheng[6] and Zhou[7, 9]. Here, the behaviour in time of the degree of branching[5, 6], the dendritic and linear units[6] and the fraction of cyclized molecules[5] has been obtained. In the work by Galina[5] and Cheng [6] the average microstructural properties have been computed using the generating functions approach. More recently, the 2-dimensional chain-length/degree-of-branching distribution was obtained in the form of an analytical expression by Zhou[7] under the assumption that no cyclization reaction takes place. The intramolecular reaction of cyclization has indeed been considered in [5]. In view of its interesting gelation behaviour, the AB_3 sys-

tem has been investigated using Monte Carlo simulation by Somvasky et al. [10] Rather than substitution they were interested in the effect of *shielding* of monomer groups, leading to a shift of the gel point to higher conversion. They deal with the steric excluded volume effect by introducing so-called exponent *kernels*, thereby mimicking non equal accessibility of reactive functional groups. In the present paper we show that our newly developed numerical method can be easily adapted to capture the shielding effect in AB_2 system employing an exponent kernel.

The new computational techniques that we will present in this paper are another contribution to the area of growing interest that is formed by the search after multidimensional distributive properties, where we previously treated polymer modification [11, 12] and crosslinking polymerization [13, 11, 12]. In the realm of this trend here we will show how multidimensional distributive properties can be recovered for the AB_2 polymerization system with substitution, cyclization, and shielding. The following reaction mechanism is considered:



where x is a number of terminal units, and y is a number of liner units in the hyperbranched polymer. The first two lines correspond to the polymerization reaction for substituted and non substituted groups. The third and forth lines denote the intramolecular reaction of cyclization. The fifth and sixth lines denote the reaction between cyclized and non-cyclized molecules. The rate coefficients are not constant, and depend on x , y , chemical substitution ratio ρ , cyclisation factor λ and scaling constant K_t . Note, that we do not yet explicitly refer to shielding in this formulation.

The paper is organised as follows.

Firstly, we discuss the main concepts of *graph theory* that has been used to describe molecular topologies of hyperbranched AB_2 polymer. Graph theory is not only an important tool to build the mathematical model that is going to be solved. It also helps us understanding the connections between different distributive properties and, in addition, it allows expressing one property in terms of the other at the post-processing stage. *Secondly*, we show how the rules of topology evolution as induced by the chemical reactions, may be transformed into mathematical balance equations. The non-linear integro-differential equations will be discretized and solved numerically employing linearisation and projection methods.

Thirdly, we demonstrate how the 'raw' numerical result, a three-dimensional distribution, may be post-processed in order to retrieve different distributive properties. The average properties and the chain length distribution obtained from the model, are shown to perfectly agree with findings of earlier investigations [5, 6, 7] for the case without cyclization. Furthermore, we show the first ever full multidimensional distributive properties for systems that experience *both* substitution and cyclization simultaneously.

Fourthly, we show how the designed numerical method can be adapted to capture the steric excluded volume effect by using the exponent kernels - the first time this concept is realized in a deterministic manner.

1. Graph representation for hyperbranched polymers

The topology of a hyperbranched polymer is now described in terms of *graph theory*. According to this approach, each monomer in the polymer of the AB_2 type has one *node* associated with it, while the chemical bonds between the monomers are represented by *edges*. A single polymer molecule is represented by a connected graph G with nodes of maximum *degree* three and at most one cycle. Moreover, the structure of a non-cyclized polymer molecule does not contain cycles at all, and is therefore called a *rooted binary tree*. In the present case of AB_2 a cyclized polymer graph has exactly one cycle, see Figure 1. Now, it is useful to distinguish monomers according to their position in the topology

graph. Table 1 shows the correspondence between monomer position, graph theory terms, and commonly used short names [5, 6].

Monomer	Graph theory term	Short name
two reacted B groups, and unreacted A	root node	<i>root, R</i>
two unreacted B groups, A reacted	node of degree one	<i>terminal unit, T</i>
one reacted and one unreacted group B , A reacted	node of degree two	<i>linear unit, L</i>
all A and B groups reacted	node of degree three	<i>dendritic unit, D</i>
polymer with no unreacted A groups	graph with a cycle	<i>cycle, C</i>

Table 1: A graph theoretical frame of reference of AB_2 polymer molecules.

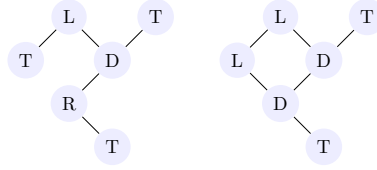


Figure 1: The graph on the left has a tree topology with root R , while the graph on the right has a cycle. The length of the cycle is equal to 4.

The graph representation brings a lot of advantages along, for instance, using basic equalities from graph theory [14] one immediately infers the connection between the parameters given in Table 1 take place. In fact, it suffices knowing only two of the parameters in order to reconstruct the others, see Figure 2.

Indeed, the dependence of the total number of units on the number of terminal and linear units is given by the rather trivial expression,

$$N = 2T + L + C - 1. \quad (1.1)$$

Now, the AB_2 polymerization process leading to branched topologies, can be viewed as a specific *random graph process* [15] that starts with n nodes and no edges, and subsequently at each step connects certain nodes according to the reactions taking place.

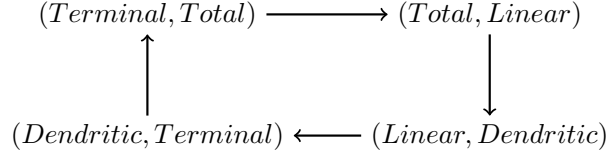


Figure 2: By knowing two of four parameters it is possible to recover the other two.

2. Reaction mechanisms and mathematical model

Let $\bar{G} = \{G\}$ be a collection of graphs (sometimes referred to as a *forest* [14]) with, possibly repeating, components of the form G . Hence, \bar{G} is a *multiset*. Employing this notation, we refer to G as to a single polymer molecule, while $s \in \bar{G}$ represents all molecules instantaneously present in the system, and \bar{G} all possible molecules that may be generated with the AB_2 polymerization process.

Following the conventional approach for AB_2 systems with substitution, two polymerization reactions[5, 6] and a cyclization[5] reaction are considered. Recalling x, y denotes amount of terminal and linear units, the interpretation of the reactions in terms of the random graph process emerges as:

- two arbitrary tree-components of \bar{G} join together by connecting the root R from one component and a terminal unit T from another at rate K_t ,

$$P_{x,y} + P_{x',y'} \rightarrow P_{x+x'-1,y+y'+1};$$

- two arbitrary tree-components of \bar{G} (at least one of two is not strictly binary) join together by connecting the root R from one tree and a linear unit L from another at rate ρK_t ,

$$P_{x,y} + P_{x',y'} \rightarrow P_{x+x',y+y'-1};$$

- an arbitrary tree component of \bar{G} receives a cycle by connecting the root R with a terminal unit T at rate λK_t or by connecting root R and linear unit L at rate ρK_t ,

$$P_{x,y} \rightarrow C_{x-1,y},$$

$$P_{x,y} \rightarrow C_{x,y-1};$$

- two arbitrary tree-components of \bar{G} , of which one possesses a cycle, join together by connecting a root R from one molecule and a terminal unit T from another at rate K_t ; or join by connecting root the R from one tree and a linear unit L from another at rate ρK_t ,

$$P_{x,y} + C_{x',y'} \rightarrow P_{x+x'-1,y+y'+1},$$

$$P_{x,y} + C_{x',y'} \rightarrow P_{x+x',y+y'-1}.$$

Suppose we have a system of polymers s . Let each graph $g \in G$ has a number $0 \leq F_s(g) \leq 1$ associated with it that corresponds to the relative frequency of occurrence of graph g within the system $s \in \bar{G}$. In other words, for each selected topology g , $F_s(g)$ tells how probable it is finding g within a particular system s . As g contains full information on molecular topology, it is important to note that the whole system s , consisting of a large number of molecules, would have to be represented by an ensemble of the above-described graphs, which would require a huge amount of data to store. Thus, we will rather distinguish topologies only by three parameters (T, L, C) , mapping $G \rightarrow \Omega \times \{0, 1\}$, $\Omega = [0, \infty)^2$. Here Ω denotes the domain of all possible values for parameters (T, L) . On the other hand, we expect s to be exclusively dependent on time by considering a function $s(t)$. This reduces the original measure $F_{s(t)}$ to

$$f_c(x, y, t) \in W, \quad c \in \{0, 1\}, \quad (2.1)$$

which denotes the relative frequency of occurrence of a connected component with a number of terminal units between x and $x + dx$, a number of linear units between y and $y + dy$, and c cycles in the polymerization system at time t . We refer to $W = L^2(\Omega) \times C[1, \infty)$, as a short way to describe mathematical properties of the distribution $f(x, y, t)$. Namely, $L^2(\Omega)$ suggests $f_c(x, y, t)$ is

integrable over the first two variables x, y ; $C[1, \infty]$ mark it is continuous in time, t . We will deliberately use this shortening in the paper. For instance, when referring to a mapping $W \rightarrow W$, a law that sets correspondence between two distributions from W ; a mapping $W^2 \rightarrow W$ - correspondence between a pair of distributions and another distribution from W ; and $W \rightarrow \mathbb{R}$ - correspondence between a distribution for W and a real number.

Passing to the limit $dx, dy \rightarrow 0$ the evolution of $f_c(x, y, t)$ with time may be described with a system of differential equations. Two equations are derived, for cyclized polymers $c = 1$, and for non-cyclized ones, $c = 0$,

$$\frac{\partial f_c(x, y, t)}{\partial t} = (\mathcal{L}_c f)(x, y, t), \quad c = 0, 1 \quad (2.2)$$

subject to the initial conditions

$$\begin{cases} f_0(x, y, 0) = \delta(x - 1)\delta(y), \\ f_1(x, y, 0) = 0, \end{cases} \quad (2.3)$$

where δ is a delta function and operator $\mathcal{L} : W \rightarrow W$ implements the effect of the reactions listed at the beginning of this paragraph on the distribution f_c . The operator fully determines the dynamics of the system and, as it will be shown further on, has a non-linear structure. Now, we start with a set of basic operators, typical for polymerization, that also act on f_c and eventually will serve as building blocks to define a more complicated structure of \mathcal{L} .

Definition 2.1. *The shift operator $T_{x_s, y_s} \in W \rightarrow W$ takes a function $f \in W$ to its translation $T_{x_s, y_s} f$,*

$$T_{x_s, y_s} f(x, y, t) = f(x - x_s, y - y_s, t), \quad (x_s, y_s) \in \Omega. \quad (2.4)$$

We normally associate the operator (2.4) with propagation-like reaction mechanisms, where at each firing of the reaction one node is added to the connected component G .

Example 2.1. *Let us consider a simple propagation reaction $P_{1,y} + M \xrightarrow{K_t} P_{1,y+1}$, meaning that the lengths of the linear chains $P_{1,y}$ are growing at constant*

rate K_t . The corresponding differential equation has the form

$$\frac{\partial}{\partial t} f(x, y, t) = K_t \left(T_{0,1} f(x, y, t) - f(x, y, t) \right).$$

The differential equation from Example 2.1 may be viewed as a partial case of a chemical master equation [16]. Note besides that any chemical master equation may be represented as a linear combination of shift operators (2.4).

Definition 2.2. Integral operators $\mu, \mu_x, \mu_y : W \rightarrow \mathbb{R}$, take a function f to its partial moments $\mu f, \mu_x f, \mu_y f$:

$$\begin{aligned} (\mu f)(t) &= \int_{\Omega} f(x, y, t) dx dy, \\ (\mu_x f)(t) &= \int_{\Omega} x f(x, y, t) dx dy, \\ (\mu_y f)(t) &= \int_{\Omega} y f(x, y, t) dx dy, \end{aligned} \tag{2.5}$$

Example 2.2. Let $f_c(x, y, t) \in W$ be a known evolution of the topology for an AB_2 polymerization system as described in Section 1. Then, as a direct consequence of the equality (1.1), the total mass time profile for the non-cyclized polymers ($c = 0$) is given by

$$m(t) = (2\mu_x + \mu_y - \mu) f_0(x, y, t).$$

Definition 2.3. Convolution is an operation that takes two arguments $f, g \in W$ to a product $f * g$ defined as

$$f(x, y, t) * g(x, y, t) = \int_0^x \int_0^y f(\xi, \eta, t) g(x - \xi, y - \eta, t) d\xi d\eta \tag{2.6}$$

It may easily be checked that the convolution is a *symmetrical* $f * g = g * f$, and a bilinear $a \cdot f * g = a \cdot (f * g)$, $a \in \mathbb{R}$ operation. Note, that the operation exhibits special behaviour regarding the 0-moment:

$$\mu(f * g) = \mu f \cdot \mu g \tag{2.7}$$

The convolution is an important tool when modelling step-growth polymerization [11]. Firing of such a reaction in terms of a random graph process means that any two arbitrary disconnected components from \bar{G} become connected by a new edge. This is illustrated by the following example.

Example 2.3. Let us consider a polymerization reaction described by the reaction equation $P_{x,y} + P_{x',y'} \xrightarrow{K_t} P_{x+x',y+y'}$, where the reaction rate is not dependent on x, y, x', y' . In contrast to to Example (2.1) there are multiple choices to select the reactants, so $P_{x,y}$ is produced for a fixed combination x, y . The corresponding differential equation has is formulated as,

$$\frac{\partial}{\partial t} f(x, y, t) = K_t \left(f(x, y, t) * f(x, y, t) - f(x, y, t) \cdot \mu f(x, y, t) \right).$$

The differential equation presented in Example (2.3) can be also viewed as a Smoluchowski coagulation equation [17].

Now, we are ready to define $\mathcal{L}(f_c(x, y, t))$, $c = 0, 1$, as appearing in (2.2). In analogy to the ideas expressed in Examples 2.1-2.3 we assemble the operator $\mathcal{L}_{0,1}$,

$$\begin{aligned} \mathcal{L}_0(f_c) = & K_t \left(T_{0,1} f_0 * x f_0 - (\mu_x f_0 + \mu f_0 x) \cdot f_0 - \lambda x f_0 \right) + \\ & \rho K_t \left(T_{1,-1} f_0 * y f_0 - (\mu_y f_0 + \mu f_0 y) \cdot f_0 - \lambda y f_0 \right); \end{aligned} \quad (2.8)$$

$$\mathcal{L}_1(f_c) = K_t(T_{0,1} x f_1 * f_0 - x f_1 \mu f_0) + \rho K_t(T_{1,-1} y f_1 * f_0 - y f_1 \mu f_0) + \lambda K_t(x f_0 + \rho y f_0). \quad (2.9)$$

Here as before, the subscript denotes the balances for cyclized 1 and non-cyclized 0 molecules. The equation (2.8) consists of two similar lines that correspond to $R + T$ and $R + L$ reactions. Here, $\rho > 0$ is the chemical substitution factor. As similar to Example 2.3 $T_{0,1} f_0 * x f_0$ denotes the production term. Here, however, the weight x has been used as the reaction rate is proportional to the amount of terminal units. The shift operator $T_{0,1}$ was employed, since with every reaction firing, one extra linear unit appears. The consumption term $-(\mu_x f_0 + \mu f_0 x) \cdot f_0$ shows that each polymer might participate in the reaction by contributing either an R unit at rate $\mu f_0 \cdot x f_0$ or a T unit at rate $\mu_x f_0 \cdot f_0$. Finally, the cyclization $R + T$ occurs at rate $\lambda K_t x f_0$, where $\lambda \geq 0$ is a constant factor. The second line of (2.8) may be analyzed in an analogous manner with as a major difference that it denotes the substituted reaction $R + L$ this time.

It may be seen that the balance equation for components without cycles (2.8) is presented in a closed form, so the differential equation for f_0 may be solved

independently of f_1 . In the case f_0 is known, f_1 may be resolved by integration

$$\frac{\partial f_1(x, y, t)}{\partial t} = \mathcal{L}_1(f_c(x, y, t)). \quad (2.10)$$

For this reason we subsequently consider two differential equations instead of the full system (2.2). The numerical approach is similar for the cases and will first be introduced for \mathcal{L}_0 .

2.1. Numerical treatment

We start with the time discretization. In view of the non-linear nature of (2.2), it is important to employ an implicit time integration scheme, also known as Rothe's method. Let $\hat{f}(x, y, t_k)$ be an approximation to f_0 , the solution of (2.2). Then, an implicit first order time integration scheme is given by

$$\hat{f}(x, y, t_{k+1}) = \hat{f}(x, y, t_k) + \tau_k \mathcal{L}_0 \hat{f}(x, y, t_{k+1}), \quad k = 0, 1, 2, \dots$$

or in a more compact way,

$$(\tau_k \mathcal{L}_0 - I) \cdot \hat{f}(x, y, t_{k+1}) + \hat{f}(x, y, t_k) = 0, \quad k = 0, 1, 2, \dots \quad (2.11)$$

where I is an identity operator and $\tau_k = t_{k+1} - t_k$ is a time step. Now, there are two main issues in solving the equation (2.11) for $\hat{f}(x, y, t_{k+1})$. On each time step we deal with:

- *Linearization*: find a linear equation that mimics the behaviour of (2.11) locally with respect to (x, y) .
- *Approximation*: find an approximate solution that satisfies the linear equation up to certain error tolerance.

Let $\mathcal{L}'_0 : W^2 \rightarrow W$ be the Frechét derivative [18] of \mathcal{L}_0 at point $f(x, y, t_k)$,

$$\begin{aligned} \mathcal{L}'_0 \hat{f} h = & K_t \left(T_{0,1} (f * xh + h * xf) - \mu_x f \cdot h - (\mu f + \lambda) x \cdot h \right) + \\ & \rho K_t \left(T_{1,-1} (f * yh + h * yf) - \mu_y f \cdot h - (\mu f + \lambda) y \cdot h \right). \end{aligned} \quad (2.12)$$

Here, the direction $h \in W$ of Frechét derivative should not be confused with the time step τ_k . Now, a functional Newton's method may be applied to (2.11)

that defines a sequence $\{\hat{f}^s\}_0^\infty$ converging to the root $\hat{f}(x, y, t_{k+1})$ of equation (2.11),

$$\hat{f}^{s+1} = \hat{f}^s - h_s. \quad (2.13)$$

Here, we assume that the time step index k is fixed and the initial estimation $\hat{f}^0(x, y, t_{k+1})$ is given. Now, with each iteration $s = 0, 1, 2, \dots$, the new estimate \hat{f}^{s+1} is obtained as an upgrade of \hat{f}^s with a certain correction term h_s that solves the equation

$$(\tau_k \mathcal{L}'_0 \hat{f}^s - I)h_s = (\tau_k \mathcal{L}_0 - I)\hat{f}^s + \hat{f}(x, y, t_k). \quad (2.14)$$

Although the equations (2.13, 2.14) contain \mathcal{L}_0 , they are linear with respect to the correction term h_s . However, the estimated solution \hat{f}^{s+1} is expressed only implicitly as shown in (2.14). Thus, we proceed by approximately solving (2.14) employing a collocation projection into a Gaussian basis[11].

Let $a(h, v) : W^2 \rightarrow \mathbb{R}$, $b(v) : W \rightarrow \mathbb{R}$ be a bilinear and a linear form, respectively, being associated with the right and left hand sides of (2.14),

$$\begin{aligned} a(h, v) &:= \langle (\tau_k \mathcal{L}'_0 \hat{f}^s - I)h, v \rangle, \\ b(v) &:= \langle (\tau_k \mathcal{L}_0 \hat{f}^s - I) + \hat{f}_{t_k}, v \rangle, \end{aligned} \quad (2.15)$$

where $\langle \cdot, \cdot \rangle$ is an inner product

$$\langle f(x, y), g(x, y) \rangle = \int_{\Omega} f(x, y)g(x, y) dx dy. \quad (2.16)$$

The equations (2.13, 2.14) may be reformulated in a *weak* sense

$$\begin{cases} \hat{f}^{s+1} = \hat{f}^s - h_s, \quad h_s \in W; \\ a(h, v) = b(v), \quad \forall v \in W. \end{cases} \quad (2.17)$$

The idea behind a 'weak' formulation is the following: instead of requiring the residual in the original equation (2.14) to be zero, we rather demand a zero inner product of the residual and all test functions $v \in W$. This is formulated in the second line of (2.17).

Finally, in order to perform the transition from the dimensionally infinite W to the finite degrees of freedom (DoF), we construct a system of n basis function

centres $(x_i, y_i) \in \Omega$ and connectivity parameters $\sigma_{.,i}$. Two n -dimensional bases in W are defined as follows

$$\phi_i(x, y) = e^{-\sigma_{x,i}(x-x_i)^2 - \sigma_{y,i}(y-y_i)^2}, \quad \sigma_{.,i} > 0, \quad i = 1, 2, \dots, n. \quad (2.18)$$

$$\psi_i(x, y) = \delta(x - x_i)\delta(y - y_i), \quad i = 1, 2, \dots, n. \quad (2.19)$$

$$W_n = \text{span}\{\phi_1, \phi_2, \dots, \phi_n\} \subset W, \quad (2.20)$$

$$W_{test} = \text{span}\{\psi_1, \psi_2, \dots, \psi_n\} \subset W, \quad (2.21)$$

The basis functions (2.18) are used for expansion of the approximation $\hat{h}, \hat{f}^s \in W_n$, where \hat{h} approximates h and, to the weak solution $h \in W$,

$$\hat{h}(x, y) = \sum_{i=1}^n \alpha_i \phi_i(x, y), \quad (2.22)$$

$$\hat{f}^s(x, y) = \sum_{i=1}^n \beta_i \phi_i(x, y), \quad (2.23)$$

while (2.19) is a source of test functions v used in (2.17). Thus, we arrive at a discrete collocation scheme for equation (2.14)

$$a(h_n, \psi_j) = b(\psi_j), \quad j = 1, 2, \dots, n \quad (2.24)$$

For the sake of brevity we write $\boldsymbol{\alpha} = (\alpha_i)$, $\boldsymbol{\beta} = (\beta_i)$ referring to the column vectors of coefficients as defined in (2.22, 2.23) and employ this matrix notation henceforth. Thus, for instance, relation (2.24) represents a system of n linear equations and by substituting (2.22) and (2.15) into (2.24) one may bring it to the following matrix form

$$M^0 \boldsymbol{\alpha} = \mathbf{b} \quad (2.25)$$

where $\boldsymbol{\alpha}$ is a column of unknown coefficients defining the approximation to the correction term \hat{h}^s , while M is a square $n \times n$ matrix,

$$\begin{aligned} M_0 &= \tau_k K_t \left(\hat{T}_{0,1} \left(C_\beta \hat{T}_x + C_{\hat{T}_x \beta} \right) - \hat{\mu}_x \boldsymbol{\beta} I_n - (\hat{\mu} \boldsymbol{\beta} + \lambda) \hat{T}_x \right) + \\ &+ \tau_k \rho K_t \left(\hat{T}_{1,-1} \left(C_\beta \hat{T}_y + C_{\hat{T}_y \beta} \right) - \hat{\mu}_y \boldsymbol{\beta} I_n - (\hat{\mu} \boldsymbol{\beta} + \lambda) \hat{T}_y \right) - I_n. \end{aligned} \quad (2.26)$$

Here, I_n is an identity matrix of size n ,

$$\hat{T}_{x_s, y_s} = A^{-1} A_{x_s, y_s} \quad (2.27)$$

is a discrete approximation to the operator (2.4),

$$\begin{aligned} (A)_{i,j} &= \phi_j(x_i, y_i) \\ (A_{x_s, y_s})_{i,j} &= \phi_j(x_i - x_s, y_i - y_s) \end{aligned}, \quad i, j = 1, 2, \dots, n \quad (2.28)$$

Matrices

$$\begin{aligned} \hat{T}_x &= A^{-1} \text{diag}\{x_1, x_2, \dots, x_n\} A, \\ \hat{T}_y &= A^{-1} \text{diag}\{y_1, y_2, \dots, y_n\} A \end{aligned} \quad (2.29)$$

represent the multiplication with weights x or y , respectively. Matrices C_β , $C_{\hat{T}_w \beta}$ represent the convolution with the known approximation \hat{f}^s or its weighted form $w\hat{f}^s$ associated to the s -th iteration of the Newton process (2.13) on the k -th time step.

$$\begin{aligned} C_\beta &= A^{-1} C, \\ (C)_{i,j} &= \sum_{k=1}^n \beta_k \phi_j(x_i, y_i) * \phi_k(x_i, y_i). \end{aligned} \quad (2.30)$$

Analogously to (2.26), by expanding (2.15) the column vector at the right-hand-side of (2.25) may be obtained as a matrix expression

$$\begin{aligned} \mathbf{b} &= \left(2\tau_k K_t \left(\hat{T}_{0,1} C_\beta \hat{T}_x - \mu_x \beta I_n - (\mu \beta - \lambda) \hat{T}_x \right) + \right. \\ &\quad \left. + \tau_k \rho K_t \left(\hat{T}_{1,-1} C_\beta \hat{T}_y - \mu_y \beta I_n - (\mu \beta - \lambda) \hat{T}_y \right) - I_n \right) \beta + \beta_{t_k}, \end{aligned} \quad (2.31)$$

Finally, the partial moments $\mu_x^k(t)$, $\mu_y^k(t)$ of the approximated distribution may be obtained by the relation

$$(\mathbf{q})_i = \int_{\Omega} \phi_i(x, y) dx dy, \quad (2.32)$$

$$\begin{aligned} \mu_x^k(t) &= \mathbf{q}^T T_x^k \beta. \\ \mu_y^k(t) &= \mathbf{q}^T T_y^k \beta. \end{aligned} \quad (2.33)$$

The considerations expressed so far show how the approximation to the distribution $f_0(x, y, t)$ of cyclized molecules may be retrieved by solving the differential equation involving \mathcal{L}_0 . The situation regarding $f_1(x, y, t)$ is even

simpler as the differential equation (2.10) has a linear form, provided f_0 is known. Thus, a linear matrix transform of the coefficient column vector $\boldsymbol{\alpha}_{t_k}$ on time step t_k is sufficient to obtain data on time step t_{k+1} .

$$\boldsymbol{\alpha}_{t_{k+1}} = \boldsymbol{\alpha}_{t_k} + \tau_k M_{\beta_{k+1}}^1 \boldsymbol{\alpha}_{t_{k+1}} \quad (2.34)$$

$$M_{\beta}^1 = 2K_t(C_{\beta}\hat{T}_x - \mathbf{q}^T\beta\hat{T}_x) + \rho K_t(C_{\beta}\hat{T}_y - \mathbf{q}^T\beta\hat{T}_y) + \lambda K_t(T_x\beta + \rho T_y\beta) \quad (2.35)$$

Until now, only a first order time integration has been considered. The numerical tools derived in the previous section may provide sufficient data for higher order time integration techniques. For instance, the computational codes belonging to multistep methods for stiff systems require subroutines computing the coefficients vector for the discretized right hand side of (2.2), $\boldsymbol{\alpha}_c = \hat{\mathcal{L}}_c\boldsymbol{\beta}$, $\hat{\mathcal{L}}_c : \mathbb{R}^n \rightarrow \mathbb{R}^n$, and its Jacobian matrix $J_{\hat{\mathcal{L}}_c}\boldsymbol{\beta}$. Here, we strongly benefit from the specific construction of the test function space (2.19, 2.21) that satisfies

$$\langle f(x, y), \psi_j(x, y) \rangle = f(x_j, y_j), \quad \psi_j \in W_{test}.$$

Furthermore, the explicit formulas for the coefficients are obtained analogously to the expressions (2.26, 2.31),

$$\begin{aligned} \hat{\mathcal{L}}_0\boldsymbol{\beta} &= \left(2K_t \left(\hat{T}_{0,1}C_{\beta}\hat{T}_x - \mu_x I_n - \mu\hat{T}_x \right) + \right. \\ &\quad \left. + K_t' \left(\hat{T}_{1,-1}C_{\beta}\hat{T}_y - \mu_y I_n - \mu\hat{T}_y \right) \right) \boldsymbol{\beta}; \\ J_{\hat{\mathcal{L}}_0}\boldsymbol{\beta} &= 2K_t \left(\hat{T}_{0,1} \left(C_{\beta}\hat{T}_x + C_{\hat{T}_x}\boldsymbol{\beta} \right) - \mu_x I_n - \mu\hat{T}_x \right) + \\ &\quad + K_t' \left(\hat{T}_{1,-1} \left(C_{\beta}\hat{T}_y + C_{\hat{T}_y}\boldsymbol{\beta} \right) - \mu_y I_n - \mu\hat{T}_y \right). \end{aligned} \quad (2.36)$$

In the case of \mathcal{L}_1 the corresponding differential equation (2.10) is linear, hence

$$\hat{\mathcal{L}}_1\boldsymbol{\beta} = J_{\hat{\mathcal{L}}_0}\boldsymbol{\beta} = M_{\beta}^1. \quad (2.37)$$

In conclusion, at this stage we have developed a fully discrete set of formulas that may be implemented into computational code in a straightforward manner or treated employing existing stiff numerical integrators (e.g. *MATLAB ode13s*).

2.2. The numerical algorithm

In order to provide a summary of the instructions listed in the previous section, the numerical algorithm is depicted in the diagram of Appendix 1. The discretization techniques presented fully describe the approximated systems by a collection of column vectors $\beta_{t_k}, k = 0, 1, 2, \dots$ that correspond to each time step t_k . Regarding space approximations, the basis function centres are enumerated with a single integer number, so notwithstanding the dimensionality of two, the problem could be parametrized using a vector of n coefficients at a single time point. Furthermore, Newton's iteration process is established at every time step t_k , so we introduce an upper index s to refer to the sequence of estimations in the Newton's process: $\beta_{t_k}^s$.

Before the algorithm starts, one must set the basis parameters $x_i, y_i, \sigma_{x,y}$. This could be realized either on the basis of the previous simulations in order to refine the results in certain parts of the domain, or as a logarithmically distributed system that covers the whole domain of possible values (x, y) , $[0, x_{max}] \times [1, y_{max}]$. There is no simple way to compute optimal values for $\sigma_{x,y}$, although the parameters should be dependent on the distance between two adjustment basis functions. Since the collocation approach tends to give the smallest absolute error at the basis function centres, the approximation error could be a posteriori evaluated locally, by repeating the simulations using additional checkpoint basis functions in between the original ones. This principle is illustrated in Figure 3. The the approach of residual subsampling[19] is applied to refine the mesh.

- If the local error is greater than a certain tolerance Tol_{add} , the intermediate checkpoint node A is accepted in the new system.
- By default all original basis centres are accepted in the new system.
- If the local error in four intermediate nodes is smaller than a predefined tolerance Tol_{remove} , the original node R situated in between is not accepted into the new system.

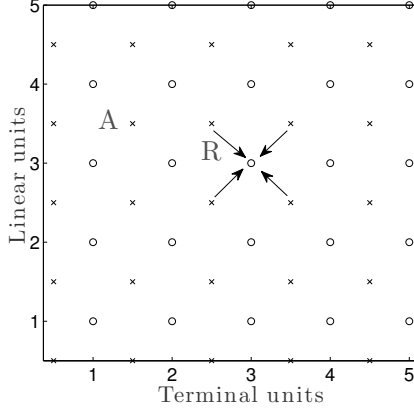


Figure 3: The principle of adaptive mesh refining is based on an error evaluation at intermediate nodes x . The original nodes system is denoted by o

The matrix expression derived in the paper could become computationally intensive. Nevertheless, as it is shown in (2.26) and (2.31), the matrices M and b , dependent on time and a certain intermediate result, are to be recomputed on every step and consist of constant numbers (2.27, 2.28, 2.29). that only depend on the fixed basis functions parameters, and hence should only be computed once at the initialization of the algorithm.

3. Results and post-analysis

The numerical scheme described in the previous paragraph shows many advantages when comparing with existing simulation techniques. It provides a representation of the full distribution, that is accurate enough to perform data mining even in the regions with very small values. Despite high precision, the method remains computationally inexpensive. As a result we are able to extract very detailed morphology related properties by post-processing. For instance information on cycle length, that was typically associated with Monte Carlo simulations before, is obtained in a fully deterministic manner.

By following the numerical scheme we generate full time profiles for non-cyclized and cyclized molecules $f_0(x, y, t)$, $f_1(x, y, t)$ that correspond to the model

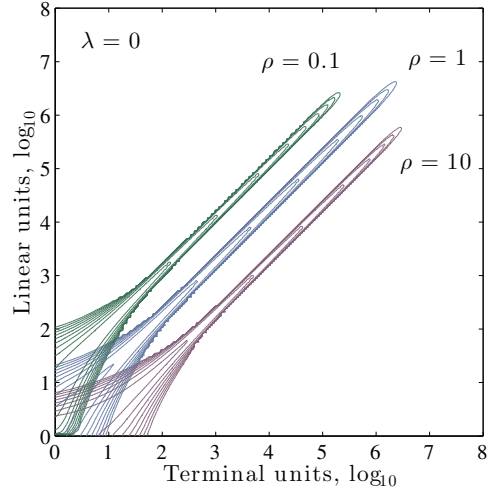


Figure 4: The level-lines of weighted frequency distribution $xyf_0(x, y, t_{end})$ as obtained from simulations. Different values for the substitution factor are considered $\rho \in \{0.1, 1, 10\}$. For each case 8 level-lines are plotted $10^{-(4.5+0.5k)}$, $k = 1, \dots, 8$.

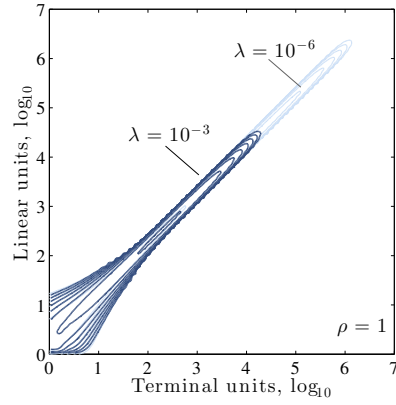


Figure 5: The level-lines of weighted frequency distribution $xyf_0(x, y, t_{end})$ as obtained from simulations. Different values for the cyclization parameter are considered $\lambda \in \{10^{-3}, 10^{-4}, 10^{-6}\}$. In each case 10 level-lines are plotted $10^{-(4.2+\frac{1}{2}k)}$, $k = 1, \dots, 8$.

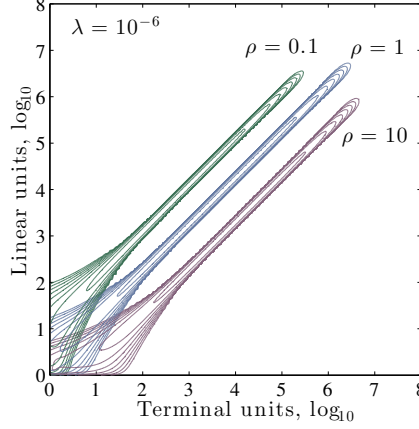


Figure 6: The level-lines of cyclized molecules frequency weighted distribution $xyf_1(x, y, t_{end})$ as retrieved from $f_0(x, y, t)$. Different values for the substitution factor are considered $\rho \in \{0.1, 1, 10\}$. In each case 7 level-lines are plotted $10^{-(5+\frac{1}{2}k)}$, $k = 1, \dots, 10$.

ρ	0.1, 1, 10
λ	0, 10^{-6} , 10^{-5} , 10^{-4} , 10^{-3}
Conversion of A groups, c	0.9, 0.99, 0.997, 0.998, 0.999, 0.9999
Degree of freedom for approximation	1200
x_i, y_i	$\{1, 2, 3, 2^k, k = 2 \dots 8 \log_2 10\}$
$\sigma_{x,i}$	$\{2.7(x_i - x_{i-1})^{-2}, i = 1, \dots, n\}$
Tolerance for Newton iterations ϵ	10^{-14}
Initial time step	10^{-10}
computational time, single core CPU:	
for quadratures (to be done once)	35 min.
for time integration (to be done for each parameter setup)	5 min.

Table 2: Parameters used in simulations

(2.2) up to a conversion of A groups $c = 99.95\%$. The full set of parameters is given in Table 2. The effect of two input parameters is studied in detail:

- ρ the ratio between the reactivity of substituted and non-substituted groups, see Figure 4;
- λ the ratio of the cyclization rate to the polymerization rate, see Figure 5.

The distribution for cyclized structures $f_1(x, y, t)$ is retrieved by integrating (2.10), Figure 6.

The results shown in Figures 4,6 already provide an idea how the substitution factor ρ influences the topologies. Indeed, varying the values for ρ is observed shifting the two dimensional distribution diagonally along the diagonal line $\log x + \log y = \text{const}$. This equally holds for non-cyclized molecules Figure 4, and cyclized molecules Figure 6. The cyclization factor λ shifts the distribution along $\log x - \log y = \text{const}$ as shown in Figure 5. This - at first sight uncomplicated - behaviour of the two dimensional distribution nevertheless has dramatic implications for the scalar and distributive properties that are to be inferred by post processing.

In view of high amount of statistical properties that are extractable from the simulation results f_c , we group them into four categories: time dependent scalars and 1,2,3-dimensional distributions.

3.1. Time dependent scalars

The time dependent scalars are obtained from the moments (2.5) of the density $f_c(x, y, t)$ as a convenient consequence of basic graph properties (1.1). All time dependent values will be presented with respect to conversion $c \in [0, 1)$ of the free A groups, so K_t coefficient may be chosen arbitrary. Indeed, the time dynamics for the conversion of A groups $c(t)$; the number of free A groups $n_A(t)$; the number of linear $n_L(t)$, terminal $n_T(t)$ or dendritic $n_D(t)$ units; the fraction of cycles $n_C(t)$ or the degree of branching may be expressed as follows:

$$\begin{aligned}
 c(t) &= \mu(f_0(x, y, t) + f_1(x, y, t)); \\
 n_A(t) &= 1 - c(t); \\
 n_L(t) &= \mu_y f_0(x, y, t); \\
 n_T(t) &= \mu_x f_0(x, y, t); \\
 n_D(t) &= n_T(t) - n_A(t); \\
 n_C(t) &= \mu f_1(x, y, t)/c(t); \\
 db(t) &= \frac{n_D}{n_D + 0.5n_L}.
 \end{aligned} \tag{3.1}$$

Here we illustrate the most important of the listed properties. The Frey's degree of branching[20] $db(t)$ turns out being strongly affected by the substitution

factor ρ , while the cyclization parameter λ does not influence the results significantly, Figure 7. On the other hand, the fraction of cyclized molecules $n_C(t)$ is dependant on λ but not on ρ , Figure 8. This results are in good agreement with previous findings[5, 6].

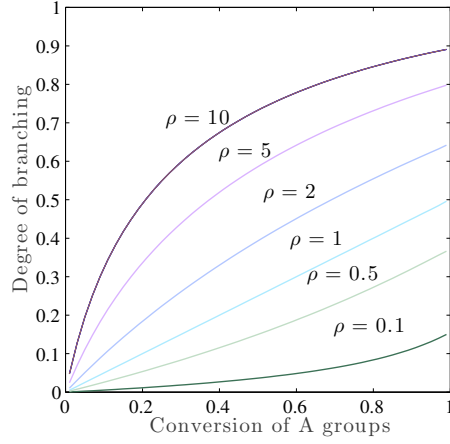


Figure 7: Degree of branching $db(t)$ as a function of conversion of A groups $c(t)$ in polymerization of AB_2 monomers reacting with a substitution effect for B-groups ρ .

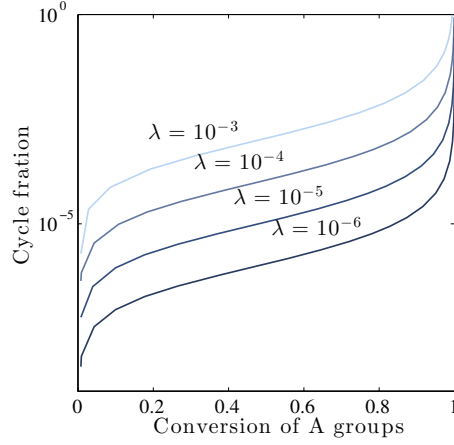


Figure 8: Fractions of cycle-containing molecules $n_C(t)$ versus conversion $c(t)$ as calculated from the simulation. The parameter λ controls the extent of cyclization. The substitution effect ρ does not affect this property.

3.2. 1-dimensional distributions

One-dimensional distributions are obtained by evaluation of line integrals of $f_c(x, y, t_{end})$ for a fixed time point t_{end} . Distributions of molecular weight, degree of branching, or cycle lengths may be obtained in this fashion by defining a collection of lines that keeps a certain property constant, see Figure 9.

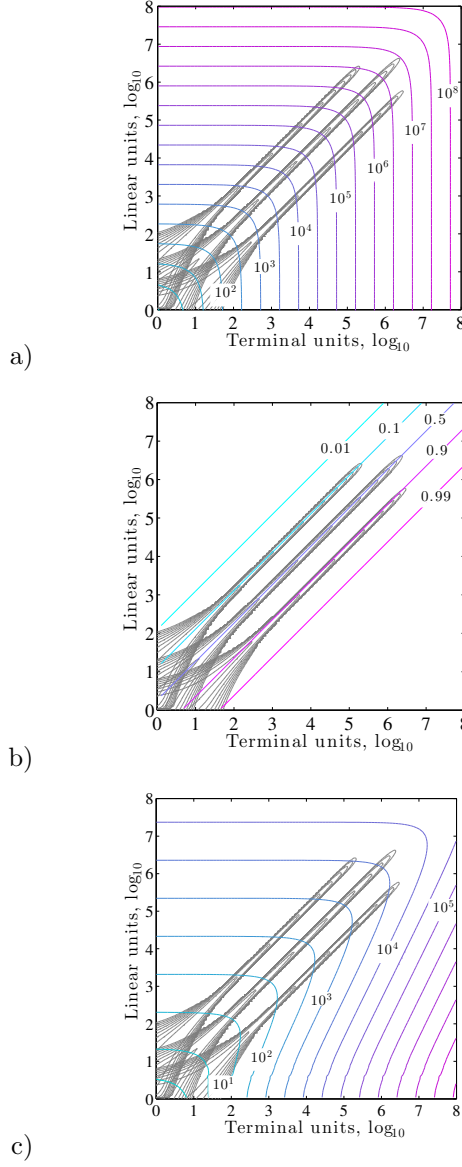


Figure 9: Three collections of lines that keep constant values of a) chain length , b) degree of branching, c) length of a cycle. The level lines of weighted frequency distribution $xyf_0(x, y, t_{end})$ with $\lambda = 0$, $\rho = \{0.1, 1, 10\}$ are plotted in the background for reference.

For instance, in order to recover the amount of molecules with a certain length n from $f_0(x, y, t_{end})$, one has to consider all combinations of points (x, y) that satisfy $2x + y - 1 = n$ (see Figure 9a), and sum the corresponding values

of f_0 . Mathematically, this is equivalent to evaluation of a line integral along the collection of lines $ld_n(y) = 0.5(n - y + 1)$, $y \in [0, n - 1]$,

$$ld(n) = \frac{1}{2} \int_0^{n-1} f_0(ld_n(y), y, t_{end}) dy \quad (3.2)$$

The molecular weight distribution $n^2ld(n)$ for various substitution factors and no cyclization is shown in Figure 10. The effect of different conversion values as the distribution is approaching its asymptotic values is shown in Figure 11. The effect of approaching a straight line in a double logarithmic plot as a system approach the gelation point was predicted before for a simpler systems[21]. It is also important to consider the cases without cyclization, as an analytical solution is known [7], which may be employed to validate the numerically obtained results. As shown in Figures 10,11 perfect agreement is observed over a span of 16 orders of magnitude.

The effect of the cyclization factor λ on the chain length distribution for a fixed conversion value and substitution factor is shown in Figure 15.

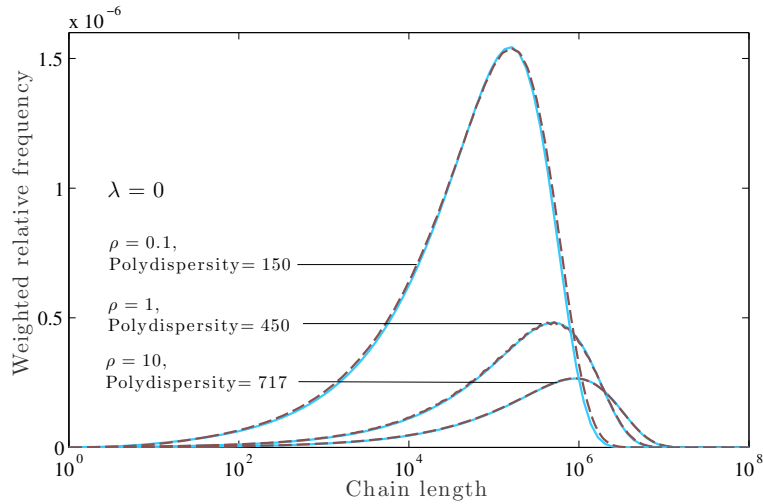


Figure 10: Normalised double weighted chain length distribution $n^2ld(n)$. The predicted values are indicated by the dashed lines and compared to the analytical solution, the solid lines. The effect of three levels of chemical substitution $\rho \in \{0.1, 1, 10\}$ is illustrated under the assumption that no cyclization takes place.

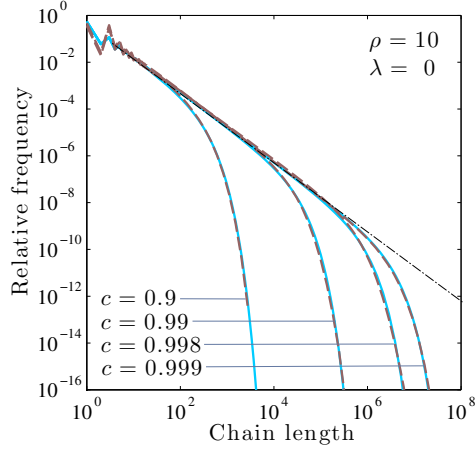


Figure 11: Chain length distribution $ld(n)$ as predicted by the numerical method, indicated by the solid lines, as compared to the analytical solution, in dashed lines. The effect of different values for conversion $c \in \{0.9, 0.99, 0.998, 0.999\}$ is illustrated under the assumption that no cyclization takes place $\lambda = 0$. The asymptotic value for conversion 1 is illustrated by the dash-dot line.

The length distributions of polymers with different degree of branching $b \in (0, 1]$ is found by integrating over the collection of lines defined by $l_b(x) = 2^{\frac{1-b}{b}}x$, $x \in [1, \infty)$ (see Figure 9b) s Analogously to (3.2) we obtain

$$bd(b) = \int_0^\infty (2x + y) f_c(x, l_b(x), t_{end}) dx. \quad (3.3)$$

Note, we intentionally use the chain length $2x + y$ as a weight while integrating in order to magnify the contribution of longer molecules, that have much more monodisperse branching distribution. Although, the weight was used we still observe prolonged tails in the branching distribution $bd(b)$ Figure 13. This fact has to be accounted for when one uses average an value instead of a distribution to describe the branched topology of the AB_2 system. We also observe that the cyclized molecules contribute less to the tails than non-cyclized molecules.

In order to obtain information concerning *cycle lengths*, we employ an idea formulated by to Panholzer et al.[22]. It was shown that the expectation of a distance $depth_{i,n}$ from the root to an i -labelled terminal unit is statistically

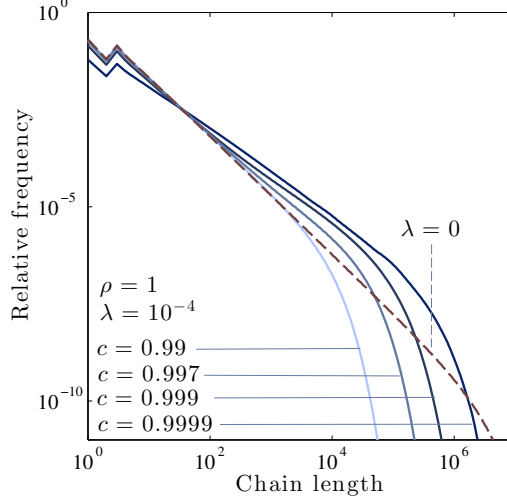


Figure 12: Chain length distribution $ld(n)$ as predicted by the numerical method. The solid lines denote cases with a cyclization factor $\lambda = 10^{-4}$, for different values of conversion. The dashed line depicts the non-cyclization case for reference. The effect of different values of conversion $c \in \{0.99, 0.997, 0.999, 0.9999\}$ is illustrated.

connected to the number of terminal units x in a *strictly binary* tree:

$$depth_{i,x} = \frac{2(2i+1)(2x-2i+1)}{x+2} \frac{\binom{2i}{i} \binom{2x-2i}{x-i}}{\binom{2x}{x}} - 1, \quad i = 0, \dots, x. \quad (3.4)$$

Now, by proportionally extending the length of each path by a number of linear units and averaging over the label index i , an expected cycle length $cl(x, y, c_{type})$ is obtained,

$$cl(x, y, c_{type}) = 2^{-c_{type}} \frac{x + 0.5y - 1}{x^2 - x} \sum_{i=0}^x depth_{i,x}. \quad (3.5)$$

The level lines of (3.5) are illustrated in Figure 9c. Note that it is important to know whether the reaction that caused cyclization added an edge between the root and a *terminal* unit $c_{type} = 0$ or between the root and a *linear* unit $c_{type} = 1$. As follows from the model (2.8), at each instant of time $\lambda(xf_0 + \rho yf_0)$ new cyclized molecules appear. The instantaneous cycle length distribution of these molecules may be extracted according to principle (3.5). In order to retrieve the total accumulated distribution of cycle lengths we have to additionally integrate

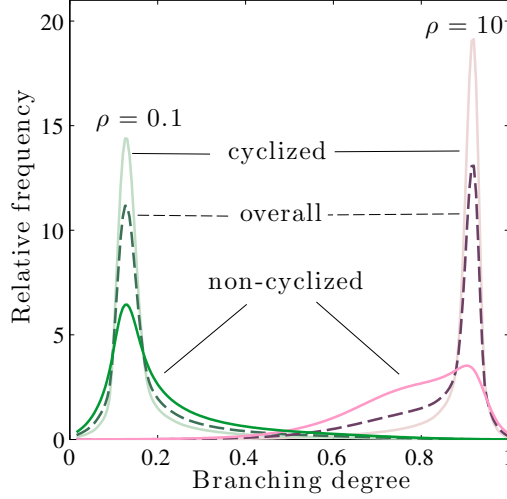


Figure 13: Normalised Frey's degree of branching distribution as obtained from the simulations for two levels of chemical substitution $\rho \in \{0.1, 10\}$. The overall distribution (the dashed lines) is plotted together with its two components, the distributions for cyclized and non-cyclized polymers (solid lines). The rate of cycle formation is $\lambda = 10^{-4}$.

over the whole time span $[0, t_{end}]$. This requires the evaluation of the double integral,

$$cd(n) = \int_0^{t_{end}} \int_{cl(x,y,0)=n} \lambda x f_0(cl(x,y), \tau) d(x,y) d\tau + \int_0^{t_{end}} \int_{cl(x,y,1)=n} \lambda \rho y f_0(cl(x,y), \tau) d(x,y) d\tau. \quad (3.6)$$

As in previous cases we evaluate the results (3.6) in a numerical manner. The result is depicted in Figure 14. That it turns out to be possible to retrieve the cycle length distribution proves the great potential of this deterministic method, especially when taking the few dimensions considered into account. It provides sufficient information to obtain morphology related properties that are usually only attainable with Monte Carlo simulations.

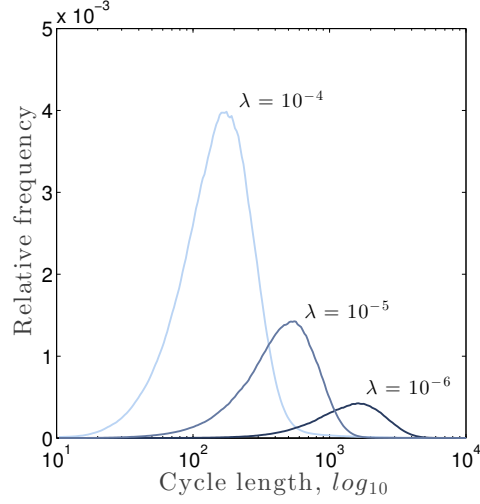


Figure 14: Normalised cycle-length distribution as obtained from the integration of $f_c(x, y, t_{end})$. The effect of different values for cyclization factor $\lambda \in \{10^{-6}, 10^{-5}, 10^{-4}\}$ is illustrated.

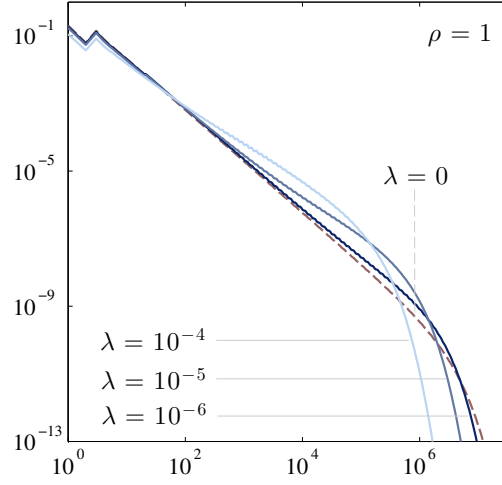


Figure 15: The effect of the different rates of cycle formation $\lambda \in \{10^{-6}, 10^{-5}, 10^{-4}\}$ on the chain length distribution. The dashed line depicts the case without cycle formation.

3.3. 2-dimensional distributions

The distribution $f_c(x, y, t_{end})$ denotes the relative frequency of structures with x terminal units, y linear units, and $c \in \{0, 1\}$, as depicted in Figures 4,6.

It is interesting to change the coordinate system of terminal units versus linear units (x, y) to another system. For instance, the coordinate system chain length versus degree of branching (d, n) may provide information that would remain unnoticed otherwise. In this case the following transformation of coordinates is required,

$$\begin{aligned} x &\rightarrow \frac{x}{x+0.5y} \\ y &\rightarrow 2x + y - 1 \end{aligned} \tag{3.7}$$

According to (3.1) the first line of the coordinates transform replaces x with Frey's degree of branching, while the second line replaces y with chain length. The resulting distribution is depicted in Figure 16. One may observe that the distributions are centred around the average property: Frey's degree of branching. However, they remain fairly broad for chain lengths smaller than 10^3 , while accompanied by extremely narrow peaks for longer chain lengths. This fact remains hidden when only the average degree branching is considered.

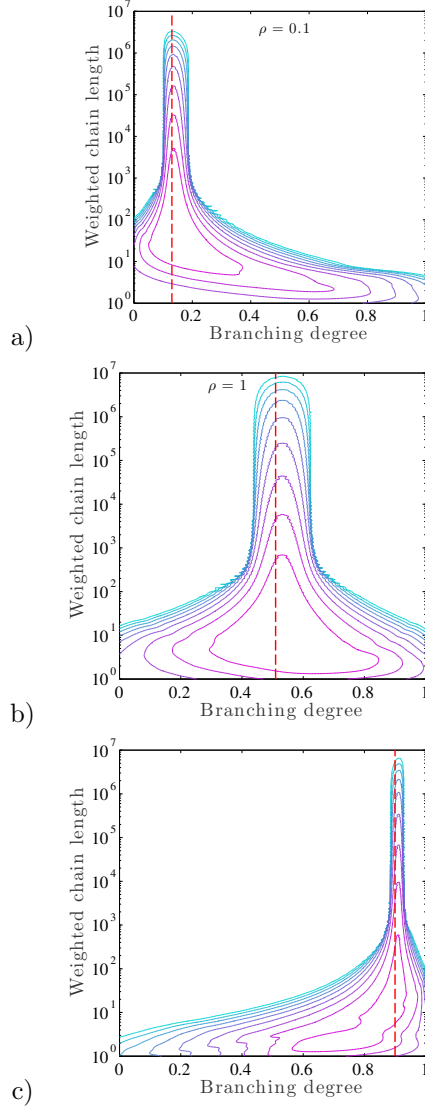


Figure 16: Two-dimensional distributions of chain length and degree of branching. Three values for the substitution factor are considered, $\rho \in \{0.1, 1, 10\}$. In each case 8 level lines are plotted, $10^{-(3+\frac{1}{2}k)}$, $k = 1, \dots, 8$. The dotted line depicts a scalar degree of branching for the whole system.

3.4. Dynamic evolution of 2D distributions

As an example of 3-dimensional distribution obtained from the simulations, we present a time trajectory for distributions shown in Figure 16. Here $f_c(x, y, t)$ is not only considered at the end time point t_{end} but similar to (3.1) on the whole

time interval $t \in [0, t_{end}]$ as depicted in Figure 17. Note, as in the previous subsection we use double-weighted chain length in order to highlight the long molecules present at extremely low concentrations.

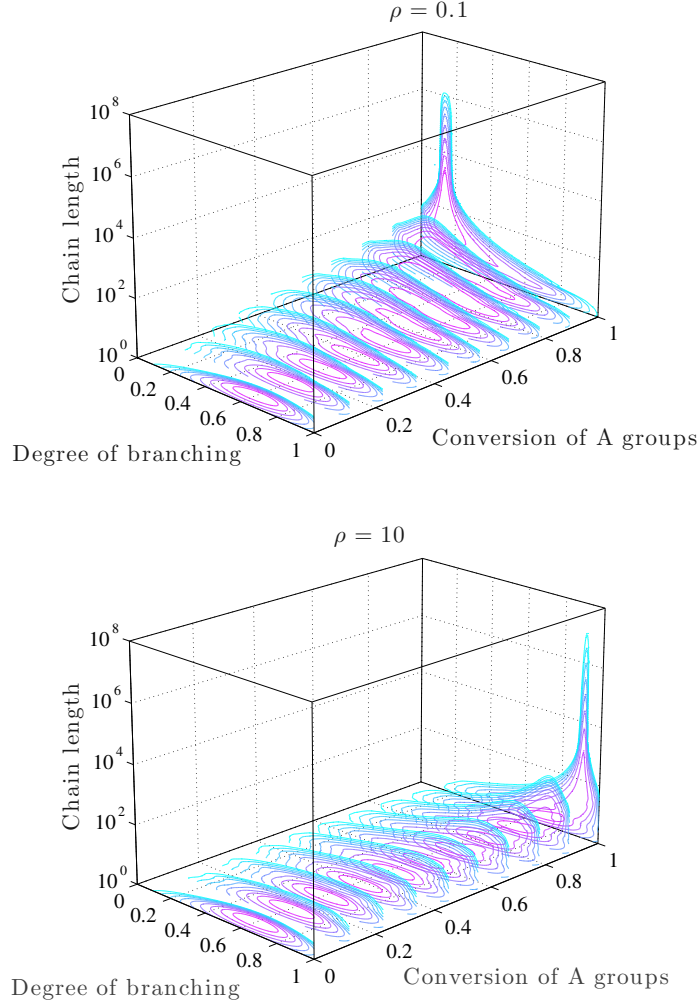


Figure 17: Molecular structures with different degree of branches and molecular weight distribution at 10 time-slices. Two values for the substitution factor are considered, $\rho \in \{0.1, 10\}$. In each case 10 level lines are plotted, $10^{-(2+0.5k)}$, $k = 1, \dots, 10$.

4. Non-linear substitution as a consequence of shielding

As has been pointed out by Šomvarsky et. al. [10, 23] the reactivity of a functional group may be dependant on the position of the group within the molecule's topology due to a steric excluded volume effect. The amount of non-shielded terminal x' and linear y' units may be defined by employing a power law

$$\begin{aligned} x' &\propto x^\omega; \\ y' &\propto y^\omega, \end{aligned} \tag{4.1}$$

where ω is the constant that describes the shape of the molecules, as a measure for the reactive surface having a fractal character [10]. The qualitative investigation of the kernels with fractional and integer values for ω has been performed by Wattis [21]. The exactly solvable cases correspond only to integer values for ω [21]. In case of a fractional ω , the method of generating functions[24] would be particularly difficult to apply as the transformation of the kernel into a domain of generating functions would imply a *fractional* differentiation, whose definition usually requires an integral transformation, which in this case would return the original (unsolved) problem. In the previous sections, we have already considered the case of possibly substituted, but equally accessible groups $\omega = 1$ and as we shall see further on that there are no particular difficulties to expand the approach to cases of fractional ω .

In the current paragraph the opposite marginal case of spheric particles $\omega = \frac{2}{3}$ is studied. The numerical scheme allows accounting for this shielding effect by applying only minor alterations to the original equations. It suffices reformulating the weight operators (2.29) in the following manner

$$\begin{aligned} \hat{T}_x^\omega &= A^{-1} \text{diag}\{x_1^\omega, x_2^\omega, \dots, x_n^\omega\} A, \\ \hat{T}_y^\omega &= A^{-1} \text{diag}\{y_1^\omega, y_2^\omega, \dots, y_n^\omega\} A \end{aligned} \tag{4.2}$$

By taking analogous steps as before we arrive at an approximate solution to the polymerization problem with shielded groups. The chain length distribution at different levels of conversion is presented in Figure 18. As a result, assuming

non equal accessibility for reactive functional groups leads to a slowing down of reaction rates, and consequently shorter molecules are formed.

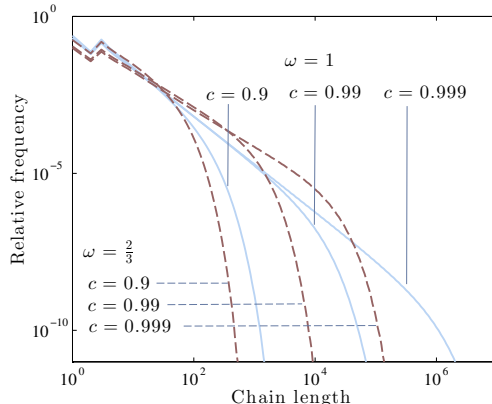


Figure 18: The chain length distributions at different levels of conversion, $c \in 0.9, 0.99, 0.999$ as obtained by numerical simulation accounting for the shielding effect, $\omega = 2/3$ (depicted with dashed line). The chain length distributions for identical parameters, but without shielding $\omega = 1$ are depicted with solid lines for reference.

Conclusions

The novel numerical method capable of capturing two-dimensional population balances rigorously, was developed as a result of clear mathematical reasoning. In contrary to prior results, the method reveals a full two-dimensional distribution. The method represents distributions as a linear combination of Gaussian basis functions, and finds their expansion coefficients, finally resulting in an approximate solution of the population balance equation. The accuracy of more than 15 orders-of-magnitude was observed when comparing with the analytical results.

The distributive properties of hyperbranched AB_2 system with a substitution has been obtained by applying the method to a population balance model. In contrast to prior modelling studies of AB_2 polymerization, the distributive properties are obtained in multiple dimensions and maintain high resolution, giving access to information of large molecules that are only present in extremely low concentrations. In addition, an intramolecular cyclization reaction has been

accounted for in the model. The influence of the chemical substitution and shielding as well as various cyclization rates on the molecular topologies has been studied.

The numerical results obtained for the case of no cyclization turned out to be in excellent agreement with the analytical solution present in the literature[7]. For the cyclization case we observe agreement with averaged properties obtained by Galina[5]. However, the newly developed method is able to reveal much more detailed information. Interestingly, the simulations show that the degree of branching is strongly dependent on the substitution factor, while the chain length is predominately determined by cyclization rate. Low cyclization rates cause small amounts of molecules with long cycle length and vice versa, high cyclization causes more molecules to have cycles, but shorter in length. It was also found that the branching distribution has a broad non-trivial shape that is non-symmetrical for cases with substitution effect. The distribution can be relatively well described by Frey’s degree of branching index (FDB) for long molecules where it deviates less from the expected value. In contrast, for short molecules the deviation increases and FDB only poorly describes topologies. It has also been observed that the degree of branching for molecules with cycles is generally more narrowly distributed than for non-cyclized molecules.

Cyclization turns out to have two different effects on the chain length distribution. Higher rates of cyclization tend to shorten the tail at very long chain length, but at the same time the chain length distribution decays more slowly in the mid range. The effect of the cyclization on chain length and branching distributions may be explained by the fact that cyclized molecules react at a lower rate, which attributes a kind of ‘memory’ to the polymerization system and blurs the distributions towards the earlier time stages.

It was also shown how the chemical substitution implemented as a linear factor, can be adapted to model the shielding effect. The shielding effect is implemented by a non-linear kernel with a fractional power, and assumes only those functional groups are accessible for reaction that are situated on the surface with dimension of fractal character.

The developed algorithm provides a fast and efficient way for predicting multidimensional distributive properties for hyperbranched polymers. This was successfully demonstrated on the example of AB_2 type polymerization accounting for the substitution effect and cyclization. Although the paper is more than just a study of a particular molecular system, we have presented a methodology that is capable of handling a wide spectrum of polymer related problems and is especially helpful in cases of more than one dimension and convolution equations.

References

- [1] W. H. Stockmayer, Theory of molecular size distribution and gel formation in branched-chain polymers, *The Journal of Chemical Physics* 11 (2) (1943) 45–55.
- [2] W. H. Stockmayer, Theory of molecular size distribution and gel formation in branched polymers ii. general cross linking, *The Journal of Chemical Physics* 12 (4) (1944) 125–131.
- [3] P. J. Flory, Molecular size distribution in three dimensional polymers. vi. branched polymers containing ab_2 type units, *Journal of the American Chemical Society* 74 (11) (1952) 2718–2723.
- [4] W. Jo, Y. Lee, Off-lattice monte carlo simulation of hyperbranched polymers, 2. effect of the reactivity ratio of linear to terminal unit on the microstructure of hyperbranched polymers based on ab_2 monomers, *Macromolecular theory and simulations* 10 (4) (2001) 225–231.
- [5] H. Galina, J. Lechowicz, M. Walczak, Kinetic modeling of hyperbranched polymerization involving an ab_2 monomer reacting with substitution effect, *Macromolecules* 35 (8) (2002) 3253–3260.
- [6] K. Cheng, T. Don, W. Guo, T. Chuang, Kinetic model of hyperbranched polymers formed by the polymerization of ab_2 monomer with a substitution effect, *Polymer* 43 (23) (2002) 6315–6322.

- [7] Z. Zhou, D. Yan, Distribution function of hyperbranched polymers formed by ab_2 type polycondensation with substitution effect, *Polymer* 47 (4) (2006) 1473–1479.
- [8] H. Galina, J. Lechowicz, M. Walczak, Model of hyperbranched polymerization involving ab_2 monomer and b_3 core molecules both reacting with substitution effect, *Macromolecules* 35 (8) (2002) 3261–3265.
- [9] Z.-p. Zhou, D.-y. Yan, Degree of branching of the hyperbranched polymers resulted from ab_2 polycondensation with substitution effect, *Chinese Journal of Polymer Science* 29 (5) (2011) 569–574.
- [10] J. Šomvársky, K. Dušek, M. Smrčková, Kinetic modelling of network formation: Size-dependent static effects, *Computational and Theoretical Polymer Science* 8 (1) (1998) 201–208.
- [11] I. Kryven, P. D. Iedema, A novel approach to population balance modeling of reactive polymer modification leading to branching, *Macromolecular Theory and Simulations* 22 (2) (2013) 85–85.
- [12] I. Kryven, A. Berkenbos, P. Melo, D.-M. Kim, P. D. Iedema, Modeling crosslinking polymerization in batch and continuous reactors, *Macromolecular Reaction Engineering* (2013) DOI: 10.1002/mren.201200073.
- [13] P. Iedema, Investigating the architecture of segmented and branched polymers under random scission by mathematical modeling, *Macromolecular Theory and Simulations* 12 (3) (2012) 187–208.
- [14] R. Diestel, *Graph Theory*, Vol. 173 of Graduate Texts in Mathematics, NY, Springer, 2000.
- [15] P. Erdős, A. Rényi, On the evolution of random graphs, *Mathematical institute of the Hungarian academy of sciences* 5 (1960) 17–61.
- [16] D. Gillespie, The chemical langevin equation, *The Journal of Chemical Physics* 113 (2000) 297–306.

- [17] M. Smoluchowski, Drei vortrage uber diffusion, brownsche bewegung und koagulation von kolloidteilchen, *Zeitschrift fur Physik* 17 (1916) 557–585.
- [18] K. Chang, *Methods in nonlinear analysis*, Springer, NY, 2005.
- [19] T. A. Driscoll, A. R. Heryudono, Adaptive residual subsampling methods for radial basis function interpolation and collocation problems, *Computers & Mathematics with Applications* 53 (6) (2007) 927–939.
- [20] D. Hölder, A. Burgath, H. Frey, Degree of branching in hyperbranched polymers, *Acta Polymerica* 48 (1-2) (1997) 30–35.
- [21] J. A. Wattis, An introduction to mathematical models of coagulation–fragmentation processes: a discrete deterministic mean-field approach, *Physica D: Nonlinear Phenomena* 222 (1) (2006) 1–20.
- [22] A. Panholzer, H. Prodinger, Moments of level numbers of leaves in binary trees, *Journal of statistical planning and inference* 101 (1) (2002) 267–279.
- [23] J. Šomvársky, K. Dušek, Kinetic monte-carlo simulation of network formation, *Polymer Bulletin* 33 (3) (1994) 369–376.
- [24] M. R. P. Costa, R. Dias, Prediction of mean square radius of gyration of tree-like polymers by a general kinetic approach, *Polymer* 48 (6) (2007) 1785–1801.

5. Appendix 1

